Progress In Electromagnetics Research C, Vol. 78, 93–104, 2017

A Circularly-Polarized Compact Wideband Patch Antenna Loaded by Metamaterial Structures

Mojtaba Simruni* **and Shahrokh Jam**

Abstract—In this paper a compact wideband aperture coupled microstrip patch antenna (MPA) with impedance bandwidth of 26.3% is designed. Size reduction of the radiating element and the slot in the ground plane is achieved by incorporating an interdigital capacitor (IDC) in the patch and a complementary split ring resonator (CSRR) close to the slot which offers composite right/left-hand (CRLH) antenna. An interdigital capacitor in the patch acts as series left-hand component, and the slot together with the CSRR in the ground plane acts as a left-hand parallel inductor. By this technique, the patch and slot dimensions compared with the initial designed antenna are reduced about 26.2% and 30.2%, respectively. Through cutting CSRRs with different arrangements in the ground plane, a dual frequency band antenna is designed. Finally, a compact wideband circularly-polarized (CP) MPA is proposed through imposing various perturbations in the current route in the ground plane of the antenna. The maximum gain and the impedance bandwidth of the designed CP antenna are 8.4 dBi and 25%, respectively. Two designed antennas are fabricated and tested. The measurement results confirm the simulation ones.

1. INTRODUCTION

Aperture coupled MPAs are attractive for present wireless communication systems due to different advantages including low profile, light weight, wide bandwidth, isolation of feed from radiating element and easily integrating with microwave circuits [1, 2]. On the other hand, reducing the size of the radiating element as a building block of a transceiver system is important. For this reason, many efforts have been made for compacting the antenna dimensions. Various techniques have been introduced for size reduction of MPAs such as using shorting pins and shorting plates, utilizing fractal antennas, cutting slots in the radiating element [3–6]. In addition to these methods, loading the antenna by metamaterial structures, including split ring resonator (SRR) and CSRR, provides new ways to achieve higher level of size reduction [7–10]. Dimensions of metaresonators, such as CSRR, are much smaller than the operating wavelength of the antenna which makes it a good candidate for miniaturization [11].

In this study, through inserting an interdigital capacitor in the patch and a CSRR close to the slot in the ground plane, a composite right/left-hand (CRLH) antenna is proposed, because the IDC acts as a left-hand series capacitor, and the slot together with the CSRR offer left-hand parallel inductor. The CSRR offers negative permeability. Thus if the MPA is used below the cutoff frequency of its equivalent waveguide, it proposes a negative permittivity medium. Therefore, a left-hand medium will be obtained together with CSRR [11]. The CSRR is a planar resonator which can be cut in the ground plane of the antenna.

In addition to antenna compacting, in some special applications, having CP antenna is necessary. Because of the advanced signal propagation properties, CP antenna technology offers numerous

Received 7 July 2017, Accepted 14 September 2017, Scheduled 2 October 2017

* Corresponding author: Mojtaba Simruni (m.simruni@sutech.ac.ir).

The authors are with the Department of Electrical and Electronic Engineering, Shiraz University of Technology, Shiraz 71555-313, Iran.

performance advantages over linear polarization (LP). As an example, within a Wi-Fi network, CP antenna delivers better connectivity with both fixed and mobile devices. Additionally, advanced signal propagation characteristics of CP make it more resistant to signal degradation due to inclement weather conditions. Reduction of the multipath effect and also the need for precise polarization alignment between transmitting and receiving antennas are the other benefits of utilizing CP antenna [12–16]. Many studies have been done on the CP MPAs for enhancing their radiation performance. In [17] a wideband CP MPA with impedance bandwidth of 16.5% and axial ratio bandwidth of 13.3% through using a special feeding mechanism has been designed. A triple-band CP antenna by utilizing Spidron fractal slot has been presented in [18]. The axial ratio bandwidths of this antenna in three different operating frequencies are 2.28%, 7.15% and 2.6%. A low profile coplanar waveguide-fed slot antenna with wideband circular polarization characteristics has been analysed in [19]. The impedance and axial ratio bandwidths of this antenna are 42% and 25.8%, respectively.

The main objective of this investigation is to present a compact wideband CP MPA which is useful for radar and electronic warfare applications. It is worth mentioning that in radar applications, through utilizing CP antenna the weather clutter can be suppressed, leading to the performance improvement of the system in target detection. Aperture coupling is utilized for feeding the MPA because of having low level of cross polarization [20]. This subject is very important in the design of the monopulse tracking radars in which the error of target tracking can be reduced [21].

This paper is organized into the following sections. In Section 2, a wideband aperture coupled MPA is designed at first. Then an IDC, as a left-hand series capacitor, is implemented in the patch. The slot in the ground plane acts as a left-hand parallel inductor which together with the IDC comprises CRLH MPA in the second designed antenna. In other words, the slot in the ground plane, inherently acts as a resonator and a left-hand inductor simultaneously. Further size reduction of the second antenna is done by incorporating a CSRR close to the slot in the ground plane. In Section 3, by appropriate displacement of the slot and CSRR, MPAs with different characteristics such as dual-band and circularly-polarized antenna are developed. The second and final proposed CP antennas are fabricated and tested. The measurement results are presented in Section 4.

2. PROPOSED DESIGNS

Among different feeding methods of MPAs, aperture coupling technique is used in the design of initial antenna because of extended bandwidth.

2.1. Wideband Aperture Coupled MPA with IDC

An aperture coupled MPA without IDC is designed at first. According to Fig. 1(b) (without considering IDC), the antenna has three layers; feed layer with $h_f = 0.762\,\text{mm}$, $\varepsilon_{rf}= 2.5$ (Rogers ultralam 2000, $\tan(\delta) = 0.0019$), patch layer1 with $h_{p1} = 8.6\,\text{mm}$, $\varepsilon_{rp}= 1$ and patch layer2 similar to the feed layer. Air gap is utilized as the patch substrate for increasing the antenna bandwidth. Analysis of the antenna is performed by full-wave high frequency structure simulator (HFSS) which uses finite element numerical methods. The return loss of the antenna is shown in Fig. 2 (red solid line), and its dimensions are listed in Table 1. The fractional impedance bandwidth of the antenna is 28% from 2.64 GHz to 3.5 GHz (return loss $< -10\,\text{dB}$).

To improve the features of the antenna, an IDC is introduced in the patch (Fig. 1(a)). The effect of variations of the IDC parameters on the antenna characteristics is studied in this section.

The initial meandered line slot which represents left-hand series capacitor is inserted in the center of upper semi-part of the patch, and in the first effort its dimensions are: $a_0 = a_1 = 1\,\text{mm}$, $a_2 = 8\,\text{mm}$, $b_0 = 8.75\,\text{mm}$, $d_0 = 1\,\text{mm}$ (Fig. 1(a)).

As can be seen in Fig. 2, although there is some mismatch in the return loss of the original antenna after cutting the IDC in the patch, a new resonant frequency is added. It should be noted that when each of the IDC parameters is varied, the other parameters of the antenna and the IDC remain constant.

Since the antenna acts as a one stage CRLH transmission line antenna, and also according to the equivalent circuit model (π-type) we have three resonances when $M = 1$ [7].

$$\beta p = \frac{n\pi}{M}, \quad n = 0, \pm 1 \quad \text{For } \pi\text{-type model} \tag{1}$$

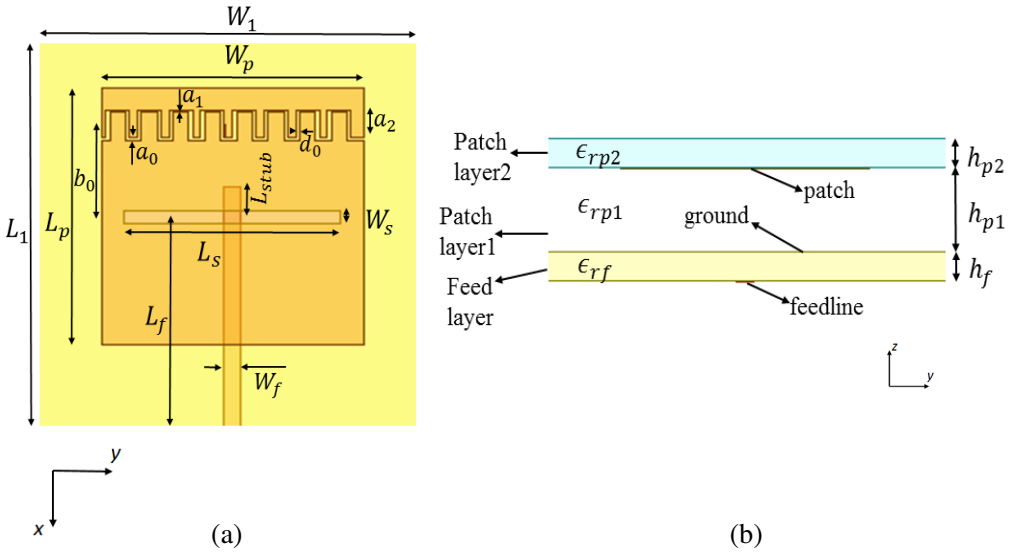

Figure 1. Aperture coupled MPA structure with the IDC. (a) Top view. (b) Side view.

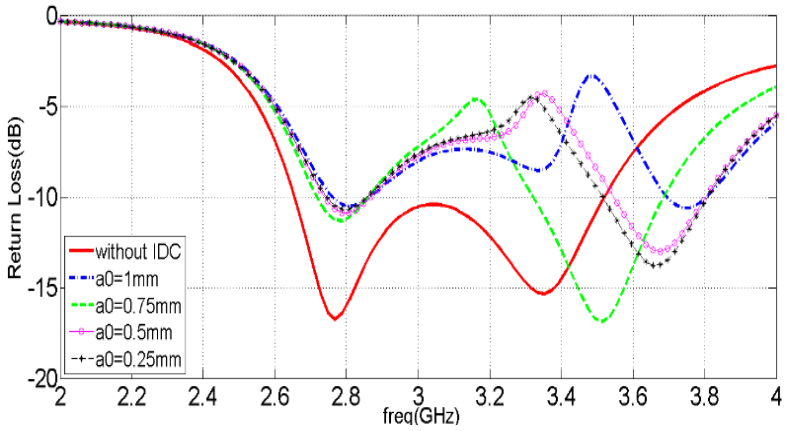

Figure 2. Simulated return loss for different a_0.

According to Fig. 2 by decreasing a_0 from 1 mm to 0.25 mm, the third resonant frequency shifts downward, whereas a_1 and a_2 are constant. The third resonant frequency is equivalent to $n = +1$. There is no change in the first resonant frequency by variation of a_0 which belongs to $n = -1$. Variation of a_1 from 0.25 mm to 1 mm has the same effect on the return loss similar to variation of a_0 that for summarization of the article; its diagrams are not presented here. Also by increasing a_2 from 5 mm to 8 mm, the third resonant frequency appears at $a_2 = 8$ mm. On the other hand, when d_0 decreases, the third resonant frequency shifts downward. Thus it can be concluded that by proper tuning of the IDC parameters, a wideband antenna can be designed through closing and mixing of three resonant frequencies.

After sweeping the IDC parameters and analyzing their effect on the return loss, the best results from each part of design, which lead to the bandwidth enhancement, are chosen. The return loss of the antenna with the optimum IDC parameters is plotted in Fig. 4(a). The antenna is wideband, and the new bandwidth is 830 MHz. Therefore, in the first step, a wideband aperture coupled MPA without IDC is designed with $BW = 28\%$ in the S-band in which the size of the patch and slot are 35 mm × 35 mm and 29 mm × 1.7 mm, respectively. Then through introducing an optimized IDC in the patch, size reduction is achieved. As shown in Fig. 4(a), after inserting the IDC, there is a small displacement in the first resonant frequency, but after compacting the radiating element, the shifting is more. The return loss

Table 1. Dimensions of initial, second and final designed (CP) antenna.

parameter	L_p	W_p	L_s	W_s	L_f	W_f	L_{stub}	a_0	a_1	a_2	d_0	b_0	h_p
Initial design values (mm)	35	35	29	1.7	50	2.15	4.7	-	-	-	-	-	8.6
second design values (mm)	34.5	30	27.2	1.7	50	2.15	4.2	0.25	0.25	2	0.5	16	8.6
final design values (mm)	33	28	27	1.3	50	2.15	4.2	0.25	0.25	2	0.5	16	8.6
parameter	h_f	L_1	W_1	L_2	L_3	L_4	L_5	L_6	L_7	L_8	L_9	L_{10}	
Initial design values (mm)	0.762	60	60	-	-	-	-	-	-	-	-	-	
second design values (mm)	0.762	60	60	-	-	-	-	-	-	-	-	-	
final design values (mm)	0.762	60	60	6	1	1	8	2	4	0.5	3.15	1	

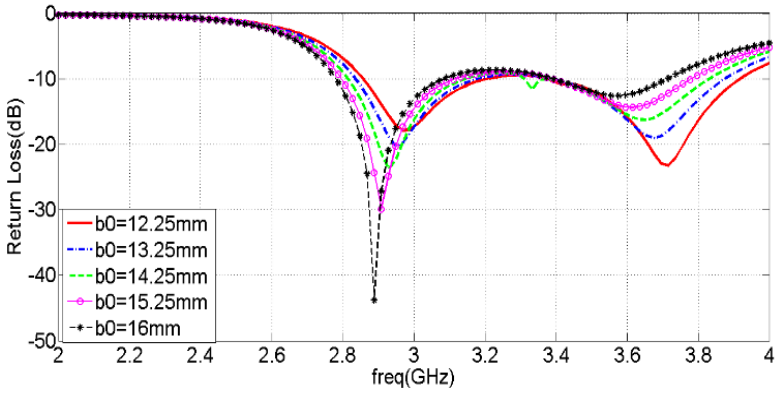

Figure 3. Simulated return loss for different b_0.

diagram of the compacted antenna must be shifted downward by changing the IDC parameters. For this reason, we set $a_2 = 2\,\text{mm}$ and move the IDC toward the radiating edge of the patch. Therefore, the resonant frequencies decrease. According to Fig. 3, the return loss diagram is shifted downward by this technique.

After size reduction, the dimensions of the patch and slot are: $34.5\,\text{mm} \times 30\,\text{mm}$ and $27.2\,\text{mm} \times 1.7\,\text{mm}$, respectively. Thus by comparing the dimensions of compacted antenna with initial design, it can

be concluded that sizes of the patch and slot are reduced in the order of 15.5% and 6.2%, respectively.

Return loss of the compacted antenna (second design) and fabricated prototype are depicted in Fig. 4(a). The simulated normalized radiation pattern at the center frequency (3 GHz) can be seen in Fig. 4(b).

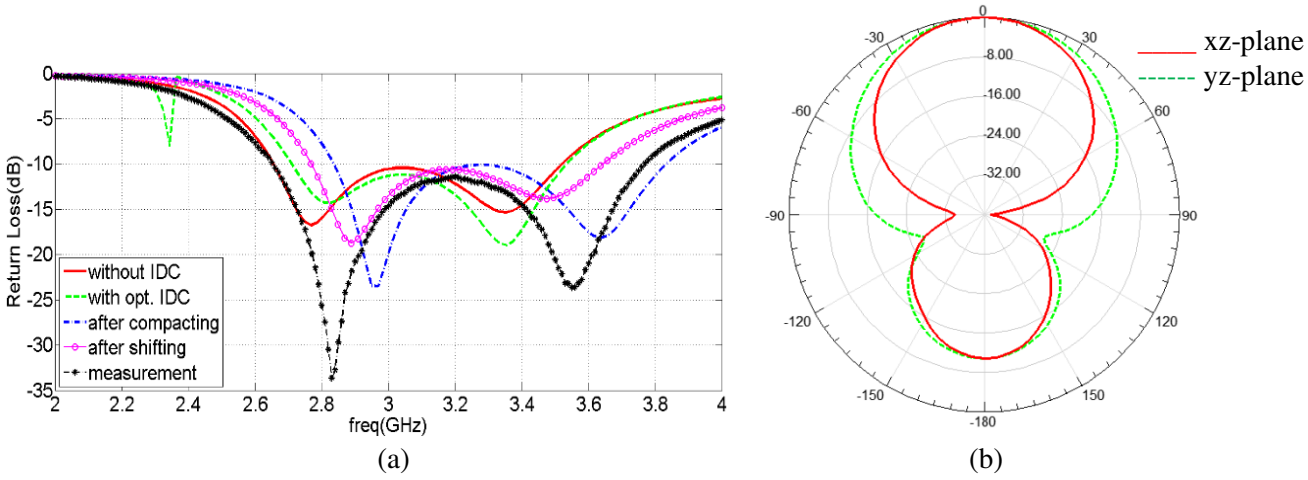

Figure 4. Antenna characteristics. (a) Return loss of the second designed antenna and the fabricated prototype. (b) Simulated normalized radiation pattern (dB) at 3 GHz.

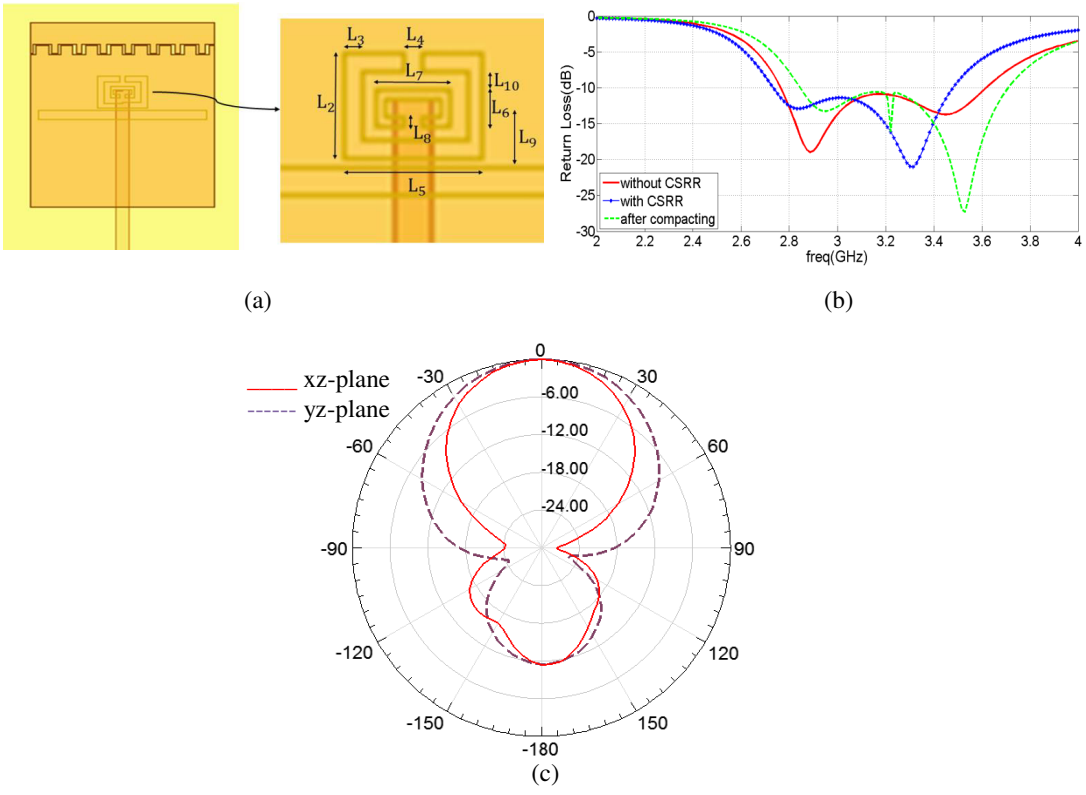

Figure 5. Proposed antenna with CSRR. (a) Top view. (b) Simulated return loss of second designed antenna (without CSRR), with CSRR and after further size reduction. (c) Simulated normalized radiation pattern (dB) of second designed MPA at 3.248 GHz.

2.2. Inserting CSRR in the Ground Plane of the Antenna

Further size reduction of the antenna is obtained through cutting a CSRR close to the slot in the ground plane of the antenna as depicted in Fig. 5(a). The equivalent circuit diagram for CSRR comprises parallel LC components which is similar to the slot's equivalent circuit model in the aperture coupled MPA [8]. Thus these two series resonators together offer a new resonator in which the resonant frequency will shift downward. Thus through further size reduction we can move the resonant frequency upward.

The simulated return losses of these antennas are demonstrated in Fig. 5(b). The fractional impedance bandwidth of the antenna is 26.3% from 2.87 GHz to 3.65 GHz. By this method, size reduction about 10.7% and 24% for the patch and slot is achieved, respectively. For comparison, the dimensions of the compacted antenna (third design) and previous designs are listed in Table 1. The simulated normalized radiation patterns of the third designed MPA in xz-plane ($\varphi = 0$) and yz-plane ($\varphi = 90$) are illustrated in Fig. 5(c).

3. CIRCULARLY POLARIZED MPA

In this section, the effects of different arrangements of CSRRs in the ground plane of the antenna are investigated. As shown in Fig. 6(a), in the first configuration, two back to face CSRRs are applied in the ground plane of the antenna. By this technique a dual-band MPA is designed (Fig. 6(b)). The resonant frequencies are at 2.91 and 3.71 GHz, and their corresponding bandwidths are 200 and 100 MHz, respectively. This antenna is linearly polarized in xz-plane. In this design, $L_9 = 5.6$ mm and all the other dimensions are similar to the antenna in Fig. 5, which are listed in Table 1. The simulated normalized radiation patterns at two frequency bands are plotted in Figs. 6(c), (d). The dual-band

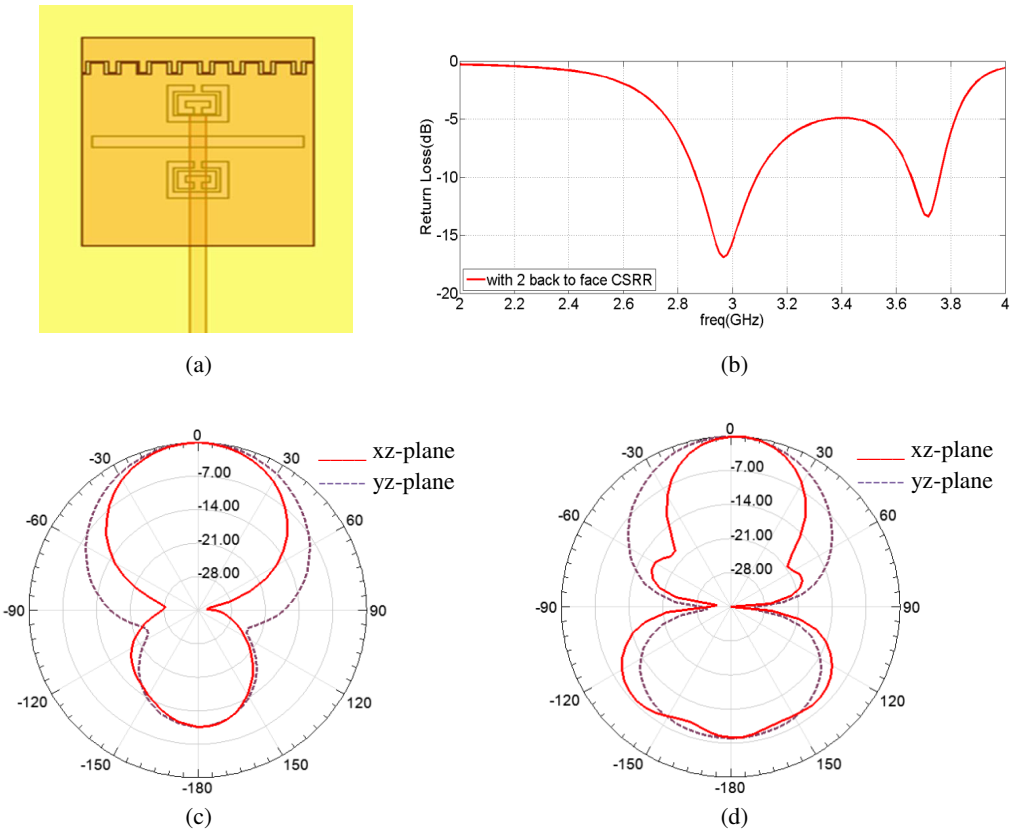

Figure 6. Forth designed antenna with two back to face CSRRs. (a) Top view. (b) Simulated returnloss (dB). (c) Simulated normalized radiation pattern (dB) at 2.96 GHz. (d) Simulated normalized radiation pattern (dB) at 3.71 GHz.

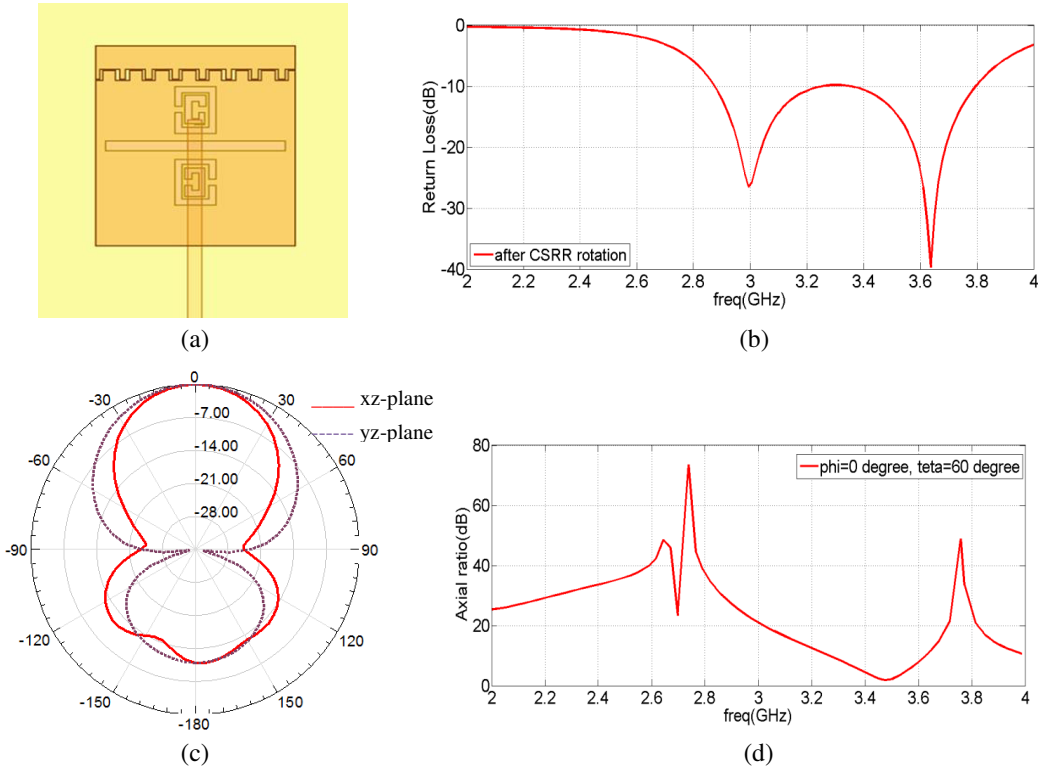

Figure 7. Proposed antenna with two 90 degree rotated CSRRs. (a) Top view. (b) Simulated return loss (dB). (c) Simulated normalized radiation pattern (dB) at 3.45 GHz. (d) Simulated axial ratio (dB).

characteristic of this antenna are useful in radar applications because the resistance of the radar against jamming systems will be enhanced. In other words, if the noise jamming occurs in the first frequency band, the radar will be able to switch the operating frequency from the first to second band.

The second arrangement of CSRRs is illustrated in Fig. 7(a). In this configuration, two CSRRs are rotated 90°. The upper one is rotated counterclockwise and the lower one clockwise. It can be revealed in Fig. 7(b) that the proposed antenna is wideband, and the fractional bandwidth is 30.4% (2.89–3.8 GHz). As demonstrated in Fig. 7(d), the antenna is circularly polarized at the frequency of 3.45 GHz (AR $<$ 3 dB). Its axial ratio bandwidth is 5.7% (Fig. 7(d)). The simulated normalized radiation pattern of the antenna is illustrated in Fig. 7(c) at 3.45 GHz.

For designing a CP antenna applying a perturbation in the current route in either the ground plane or radiating element is necessary. For this reason in the third attempt, as shown in Fig. 10(a), several changes are applied to the CSRRs, slot and the ground plane. These changes include shifting the upper and lower CSRRs to the left and right sides, respectively, rotation of the slot about 45° and incorporating a new rectangular slot in the ground plane underneath of the corner of the patch. The effect of introducing the new rectangular loop slot underneath the corner of the patch is similar to the effect of truncating triangular section from the upper corner of the patch [22]. For the purpose of better understanding the influence of the aforementioned perturbations on the performance of the MPA, parametric study is performed.

Referring to Fig. 8(a), the impedance matching at the input of the antenna varies significantly when slot's rotation angle (α) increases from 0° to 45°. The best impedance matching is obtained when $\alpha = 45°$.

Therefore, in the next steps of the design procedure we set $\alpha = 45°$. As can be seen in Fig. 8(b), through decreasing S_7, there is no considerable variation in the frequency bandwidth of the antenna. The variations of the axial ratio for different S_7 are depicted in Fig. 9. From this figure it can be comprehend that by increasing S_7, the axial ratio is decreased which means that the antenna tends to generate circularly polarized wave at the frequency of 2.89 GHz. Consequently, the final CP antenna is

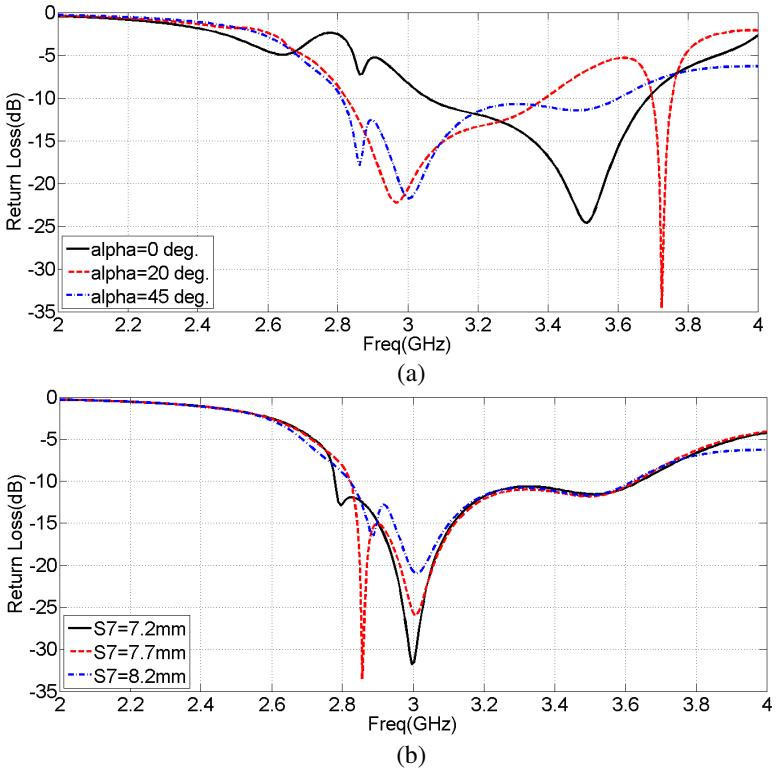

Figure 8. The effect of different perturbations on the antenna characteristics: (a) Simulated return loss for different slot's rotation angles (α). (b) Simulated return loss for different rectangular loop slot's width (S_7).

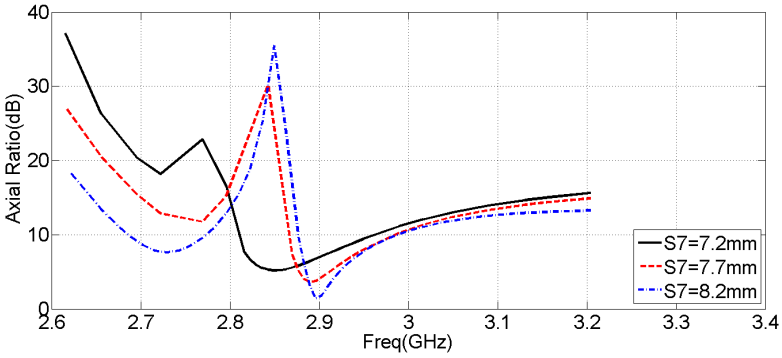

Figure 9. Simulated axial ratio for different rectangular loop slot's width (S_7).

realized when $\alpha = 45^\circ$ and $S_7 = 8.2\,\text{mm}$. According to Fig. 11(a), this antenna is wideband with the fractional impedance bandwidth of 25% from 2.8 GHz to 3.6 GHz. The displacement of the CSRRs from center to the left and right sides is 3.25 mm, and the dimensions of the rectangular slot at the corner are: $S_1 = S_3 = S_4 = 0.2\,\text{mm}$, $S_2 = 0.3\,\text{mm}$, $S_5 = 5.8\,\text{mm}$, $S_6 = 8.8\,\text{mm}$, $S_7 = 16.4\,\text{mm}$. It should be mentioned that this antenna radiates right-hand circular polarization (RHCP). If all the perturbations implemented in the ground plane for producing RHCP is mirrored along x-axis, the antenna will generate left-hand circular polarization (LHCP). The structure of this new antenna is depicted in Fig. 10(b). It should be noted that when AR $< 3\,\text{dB}$, we say that the antenna produces CP wave which is actually an approximation of elliptical polarization. Outside the axial ratio bandwidth (AR $> 3\,\text{dB}$), the elliptical polarization changes to linear polarization. It is noteworthy that the radiation efficiency of the initial

designed MPA is 95% (@2.89 GHz). After compacting the antenna by introducing the IDC and CSRR in the patch and ground plane, respectively, the radiation efficiency is reduced to 94.19% (@2.89 GHz). For final designed CP antenna, this value is 90.8% (@2.89 GHz). The comparison is performed at the frequency of 2.89 GHz in which the final proposed MPA generates CP wave.

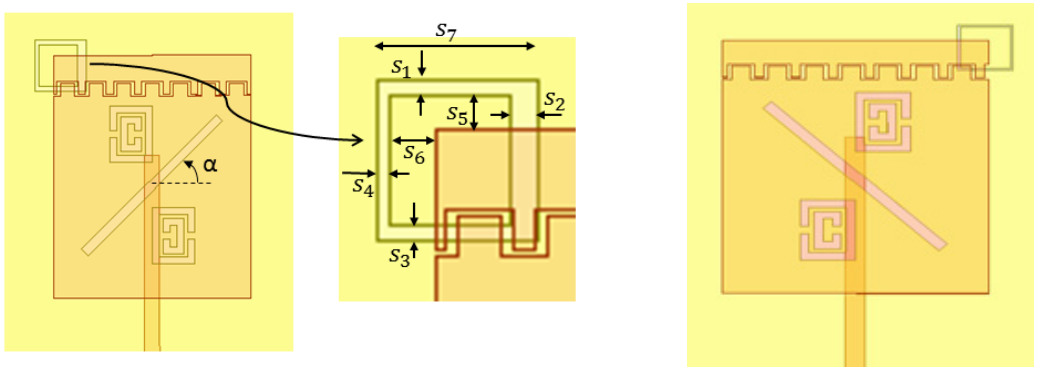

(a) (b)

Figure 10. Proposed circularly polarized antenna. (a) Top view of RHCP antenna. (b) Top view of LHCP antenna.

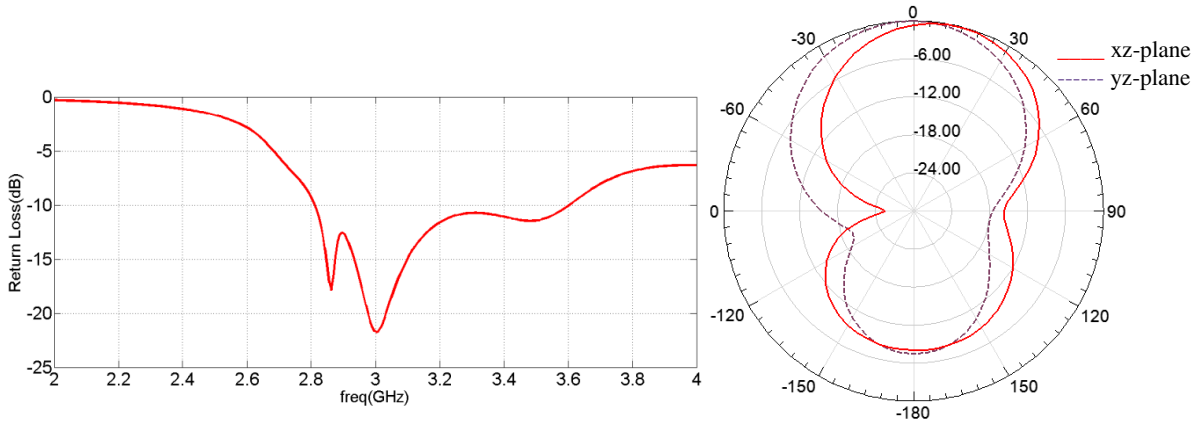

(a) (b)

Figure 11. Proposed CP antenna characteristics: (a) Simulated return loss (dB). (b) Simulated normalized radiation pattern (dB) at 2.89 GHz.

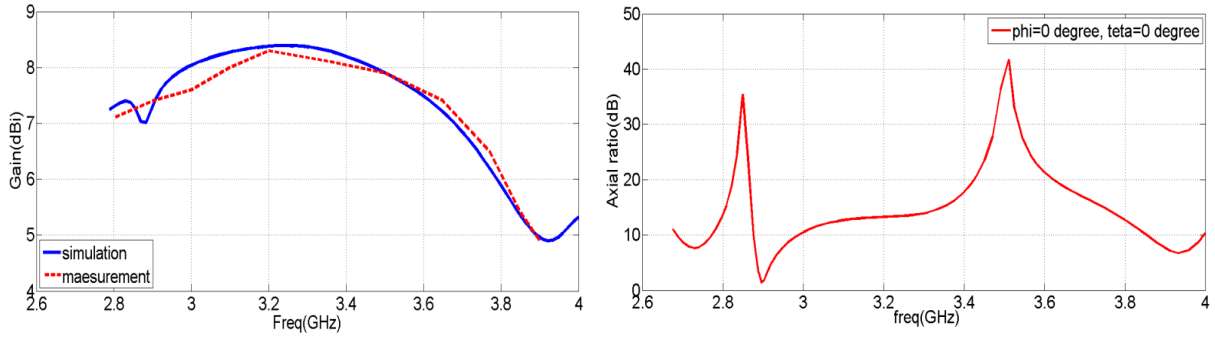

(a) (b)

Figure 12. Proposed RHCP antenna characteristic. (a) Simulated and measured gain (dBi). (b) Simulated axial ratio (dB).

According to Fig. 11(a), the proposed CP antenna has three resonant frequencies which are attributed to the slot, CSRRs and patch as different resonators. Closing these three different resonant frequencies makes contribution to the wideband characteristic of this antenna. The simulated and measured gains and axial ratio of the antenna are plotted in Figs. 12(a), (b).

4. MEASUREMENT RESULTS

In order to validate the simulation results, the second and final designed CP antennas are fabricated on a Rogers ultaralam2000 printed circuit board (PCB). According to Fig. 13(a), the patch and feed line are implemented on two separate PCBs. The air gap between the two layers is implemented by a frame of Teflon with loss tangent of 0.001. The assembled antenna can be seen in Fig. 13(b). The

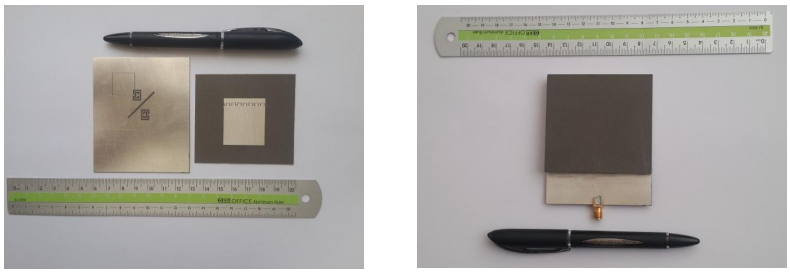

(a) (b)

Figure 13. Photograph of fabricated antenna. (a) Patch and feed boards. (b) Assembled antenna.

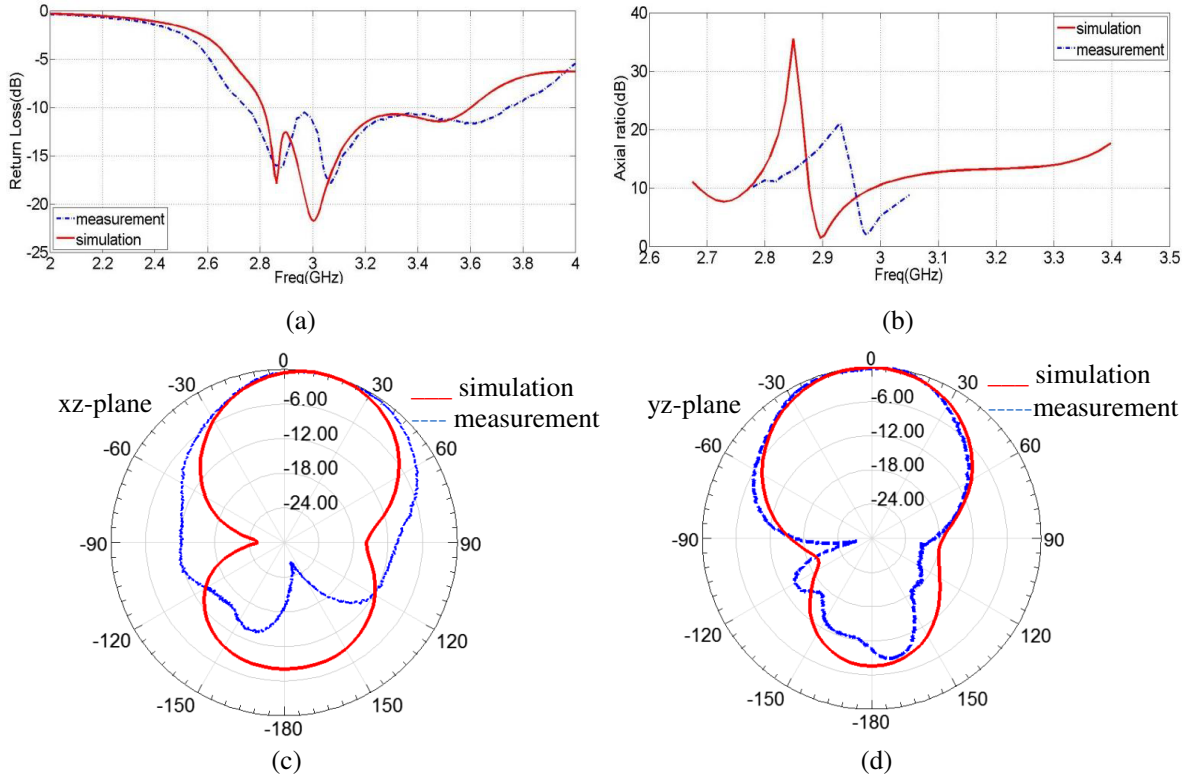

(a) (b) (c) (d)

Figure 14. Comparison between simulation and measurement results. (a) Simulated and measured return loss (dB). (b) Simulated and measured axial ratio (dB). (c) Simulated and measured normalized radiation pattern (dB) at 2.89 GHz at xz-plane. (d) Simulated and measured normalized radiation pattern (dB) at 2.89 GHz at yz-plane.

return loss of the antenna is measured by 8510C network analyzer. Comparisons between simulated and measured results for the second design and final designed (CP) antenna are illustrated in Fig. 4(a) and Figs. 14(a)–(d). There is a slight difference between simulation and measurement results due to the manufacturing tolerances and the accuracy of measurement setup. The measured return loss and axial ratio of the CP antenna are illustrated in Figs. 14(a), (b). The measured normalized radiation patterns in xz and yz-planes at the frequency of 2.89 GHz are shown in Figs. 14(c), (d). At this frequency, the antenna produces circular polarization.

As can be seen in these figures, the backlobe level of the antenna is high due to the slot radiation in the ground plane, and it can be reduced by putting an absorber or metallic reflector plate at the back of the antenna.

5. CONCLUSION

Through incorporating an IDC in the patch and a CSRR close to the slot in the ground plane of a wideband aperture coupled MPA, size reductions of the patch and slot dimensions in the order of 26.2% and 30.2% are achieved, respectively. An IDC in the patch together with the slot and CSRR in the ground plane proposes a CRLH antenna. The effect of various arrangements of CSRRs on the antenna characteristics is studied. Through this technique, a compact dual-band and a wideband MPAs are designed. By proper adjustment of two CSRRs, rotation of the slot about 45° and cutting new rectangular slot in the ground plane underneath of the corner of the patch, a wideband CP antenna is developed. By changing the situation of different perturbations in the ground plane of the antenna, switching between RHCP and LHCP is realized. The compacted antenna with the IDC and final designed RHCP antenna are fabricated and tested. Measurement results confirm the simulation results.

REFERENCES

1. Garg, R., P. Bhartia, I. Bahl, and A. Ittipiboon, *Microstrip Antenna Design Handbook*, Artech House, 2001.
2. Pozar, D. M., "A review of aperture coupled microstrip antennas: history, operation, development, and applications," Internet Archive of Univ. Massachusetts at Amherst, May 1996, archived at http:/www. ecs.umass/ece/pozar/aperture.pdf.
3. Wong, K. L., *Compact and Broadband Microstrip Antenna*, John Wiley & Sons Inc., New York, 2002.
4. Guha, D. and Y. M. M. Antar, *Microstrip and Printed Antennas New Trends, Techniques and Applications*, John Wiley & Sons Inc., New York, 2011.
5. Maza, A. R., B. Cook, G. Jabbour, and A. Shamim, "Paper-based inkjet-printed ultra-wideband fractal antennas," *IET Microwaves, Antennas & Propagation*, Vol. 6, No. 12, 1366–1373, 2012.
6. Malekpoor, H. and S. Jam, "Ultra-wideband shorted patch antennas fed by folded-patch with multi resonances," *Progress In Electromagnetics research B*, Vol. 44, 309–326, 2012.
7. Dong, Y. and T. Itoh, "Metamaterial-based antenna," *Proceedings of the IEEE*, Vol. 100, No. 7, 2271–2285, 2012.
8. Ha, G., K. Kwon, Y. Lee, and J. Choi, "Hybrid mode wideband patch antenna loaded with a planar metamaterial unit cell," *IEEE Transactions on Antennas and Propagation*, Vol. 60, No. 2, 1143–1147, 2012.
9. Mosallaei, H. and K. Sarabandi, "Antenna miniaturization and bandwidth enhancement using a reactive impedance substrate," *IEEE Transactions on Antennas and Propagation*, Vol. 52, No. 9, 2403–2414, 2004.
10. Engheta, N. and R. W. Ziolkowski, *Electromagnetic Metamaterials: Physics and Engineering Explorations*, Wiley-IEEE Press, New York, 2006.
11. Sindreu, M. D., J. Naqui, F. Paredes, J. Bonache, and F. Martin, "Electrically small resonators for planar metamaterial, microwave circuit and antenna design: A comparative analysis," *Journal of Applied Science*, Vol. 2, 375–395, 2012.

12. Qin, P. Y., A. R. Weily, Y. J. Guo, and C. H. Liang, "Polarization reconfigurable U-slot patch antenna," *IEEE Transactions on Antennas and Propagation*, Vol. 58, No. 10, 3385–3388, 2010.
13. Dong, Y., H. Toyao, and T. Itoh, "Compact circularly-polarized patch antenna loaded with metamaterial structures," *IEEE Transactions on Antennas and Propagation*, Vol. 59, No. 11, 4329–4333, 2011.
14. Vargas, D. S., F. J. H. Martinez, E. V. Munoz, L. E. G. Munoz, and V. G. Posadas, "Quad frequency linearly-polarized and dual frequency circularly-polarized microstrip patch antennas with CRLH loading," *Progress In Electromagnetics Research*, Vol. 133, 91–115, 2013.
15. Cao, W. Q., "Compact dual band dual mode circular patch antenna with broadband unidirectional linearly polarized and omnidirectional circularly polarized characteristics," *IET Microwaves, Antennas & Propagation*, Vol. 10, No. 2, 223–229, 2016.
16. Chen, C., Z. Li, L. Liu, J. Xu, P. Ning, B. Xu, X. Chen, and C. Gu, "A circularly-polarized metasurfaced dipole antenna with wide axial-ratio beamwidth and RCS reduction function," *Progress In Electromagnetics Research*, Vol. 154, 79–85, 2015.
17. Lai, H. W., K. M. Mak, and K. F. Chan, "Novel aperture-coupled microstrip-line feed for circularly polarized patch antenna," *Progress In Electromagnetics Research*, Vol. 144, 1–9, 2014.
18. Thi, T. N., S. T. Van, G. Kwon, and K. C. Hwang, "Single-feed triple band circularly polarized Spidron fractal slot antenna," *Progress In Electromagnetics Research*, Vol. 143, 207–221, 2013.
19. Chen, L., X. Ren, Y. Yin, and Z. Wang, "Broadband CPW-fed circularly polarized antenna with an irregular slot for 2.45 GHz RFID reader," *Progress In Electromagnetics Research Letters*, Vol. 41, 77–86, 2013.
20. Pirhadi, A., H. Bahrami, and J. Nasri, "Wideband high directive aperture coupled microstrip antenna design by using a FSS superstrate layer," *IEEE Transactions on Antennas and Propagation*, Vol. 60, No. 2, 2101–2106, 2012.
21. Skolnik, M. I., *Introduction to Radar Systems*, McGraw-Hill, 2001.
22. Hsu, S. and K. Chang, "A novel reconfigurable microstrip antenna with switchable circular polarization," *IEEE Antennas and Wireless Propagation Letters*, Vol. 6, 160–162, 2007.